Braz J Phys (2014) 44:697–702
DOI 10.1007/s13538-014-0264-0

SOCIEDADE BRASILEIRA DE FÍSICA

CONDENSED MATTER

Microstructure and Near Infrared Absorption of PbS Films Deposited by Chemical Bath Deposition on *p*-Type Si(100) Wafers

Rui-Fang Guo · Yan Liang · Xiao-Yong Gao · He-Jie Zhu · Sa Zhang · Hong-Tao Liu

Received: 29 June 2014 / Published online: 23 September 2014

Abstract Nanocrystalline PbS films were synthesized on *p*-type Si(100) wafers using chemical bath deposition. All of the PbS films are polycrystalline in nature with face-centered cubic (fcc) rock salt structure. The average crystallite size varied from 20 to 74 nm, thereby indicating nanocrystalline films with different molar ratios. The film composed of irregular particles was homogeneous and well adhered to the substrates. Increase in thiourea concentration from 0.5 to 2.0 M resulted into an increase in the lateral particle size and film thickness, while further increase in thiourea concentration caused a decrease in particle size and film thickness. The absorption edge of the films blueshifted slightly with increased molarities of lead sources, blueshifted initially, and then redshifted with increased molarities of sulfur sources at a fixed lead source molarities. The blueshift and redshift of the absorption edge were closely related to the change in the tensile stress of the PbS films subjected to.

Keywords PbS film · Chemical bath deposition · Molar concentration · Near-infrared absorption

R.-F. Guo · X.-Y. Gao (✉) · H.-J. Zhu · S. Zhang · H.-T. Liu
Key Laboratory of Material Physics of Ministry of Education, School of Physics and Engineering, Zhengzhou University, Zhengzhou 450052, China
e-mail: xygao@zzu.edu.cn

Y. Liang
College of Information Science and Engineering, Henan University of Technology, Zhengzhou 450001, China

1 Introduction

In recent years, film material technology has been developed by leaps and bounds and achieved remarkable results both in academic research and practical application. As a result, films, especially nanocrystalline films, are significantly interesting due to their various applications [1–5]. New effects such as the quantum-size effect can appear in the films and are hardly observed in the bulk samples [6]. Lead sulfide (PbS) belongs to groups IV–VI compound semiconductor with direct narrow band gap energy of 0.41 eV (at 300 K) and a relatively large exciton Bohr radius (18 nm) [7], which indicate potential applications of PbS in infrared detection [8, 9], photosensitive resistance, light-emitting diodes, humidity and temperature sensors, as well as decorative and solar control coatings [10, 11]. For the past few years, the properties of PbS film for various nanodevice applications have been studied. Kumar [12] used vacuum evaporation technique to prepare the high-quality polycrystalline PbS films on glass substrates and reported the characterization of these films. The structure and properties of the (001) crystal face of PbS was studied by Muscat [13] using the first-principle calculations. It is found that the linear discriminant analysis and generalized gradient approximation give results in reasonable agreement with each other, but that the structures computed with Hartree-Fock theory are vastly different. Nanda [14] investigated the band gap tuning of PbS nanoparticles by in-flight sintering of size-classified aerosols. Band gaps in the range of 0.5–2.0 eV were obtained. Li [15] reported on the ultrafast carrier dynamics and the nonlinear optical properties of PbS nanoparticles at various energy fluences. Gaiduk [16] deposited chemically nanocrystalline PbS films on Si, Ge, and GaAs substrate using alkaline solutions containing 0.05 M $Pb(NO_3)_2$, 0.04 M thiourea, 0.05 M

triethanolamine, and 0.15 M NaOH. Rutherford backscattering spectroscopy, transmission electron microscopy, and atomic force microscopy reveal that the chemical nature of the substrate has a profound influence on the structure and thickness of the deposited layers. The effect of PbS nano shell on the optical and electrical properties of PbSe core nanoparticles has been investigated by Badr [17].

Polycrystalline PbS films can be obtained by several methods such as electrodeposition [18], microwave heating [19, 20], and chemical bath deposition (CBD) [7, 21, 22]. Among these methods, CBD is more widely utilized due to its low cost, the quality of the films, and convenience for large area deposition. Although the effect of the parameters of CBD such as pH value, deposition temperature, and time, etc. on the feature (crystallite size, film thickness, etc.) of PbS films deposited on glass slides has been widely studied, effect of precursors' concentration on the microstructure and near infrared absorption properties of PbS films deposited on *p*-type Si wafers by CBD method is rarely reported. In the present investigation, we have prepared nanocrystalline PbS films on one side-polished *p*-type heavily doped Si (100) wafers with the use of different molar concentrations of lead and sulphur sources (C_{Pb} and C_S) by CBD and studied the effect of C_{Pb} and C_S on the structure and near infrared absorption of the films. It is easy to achieve compatibility with silicon electronics integration technology to grow PbS films on silicon wafers. This work will provide important support for the further fabrication of silicon-based PbS film infrared detector.

2 Experiment

2.1 Synthesis of PbS Films

Nanocrystalline PbS films were synthesized on one side-polished heavily doped *p*-type Si(100)wafers with resistivities ranging from $10^{-3}\Omega$·cm to $10^{-2}\Omega$·cm. The wafers were cleaned with traditional RCA method and then ultrasonically cleaned. Approximately 50 mL of the complex solution (pH = 10) that comprised lead acetate ($Pb(CH_3COO)_2$), thiourea ($SC(NH_2)_2$), triethanolamine (TEA), ammonia liquor ($NH_3{\cdot}H_2O$), and deionized water was placed into the reaction bath in advance. The complex solution was prepared by addition of TEA into the lead acetate solution; thiourea and ammonia liquor were then added to the resultant solution. Table 1 shows the precursor concentrations in the complex solution. Clean Si wafer was vertically immersed in the reaction bath and reacted at 350 K for 4 h. Lead acetate, thiourea, TEA, and ammonia liquor were used as Pb precursor, sulfur precursor, complexing agent, and pH modifier, respectively. Following the chemical bath reaction, the Si wafer coated with PbS film was thoroughly recleaned with deionized water for several minutes and then air dried. In the present work, two series of nanocrystalline PbS films were deposited at different C_S and fixed C_{Pb} values of 0.5 and 1.0 M.

Table 1 Precursor's concentrations in the complex solution

Sample no.	$Pb(CH_3COO)_2$ (M)	$SC(NH_2)_2$ (M)	TEA(M)	$NH_3{\cdot}H_2O$(M)
1	0.5	0.5	6.4	13.8
2	0.5	1.0	6.4	13.8
3	1.0	0.5	6.4	13.8
4	1.0	1.0	6.4	13.8
5	1.0	2.0	6.4	13.8
6	1.0	3.0	6.4	13.8

During the chemical bath reaction, the formation of PbS film depended on the rate of release of Pb^{2+} and S^{2-} from the bound state. TEA is an efficient complexant that preferably yields $[Pb(TEA)]^{2+}$, thereby reducing the concentration of free Pb^{2+} below the level required to precipitate solid $Pb(OH)_2$ [23]. PbS formation is described by the following reactions [24]

$$Pb^{2+} + TEA \rightleftharpoons [Pb(TEA)]^{2+} \quad (1)$$

$$SC(NH_2)_2 + OH^- \rightarrow HS^- + CH_2N_2 + H_2O \quad (2)$$

$$HS^- + OH^- \rightarrow S^{2-} + H_2O \quad (3)$$

$$Pb^{2+} + S^{2-} \rightarrow PbS \quad (4)$$

First, TEA reacted with Pb^{2+} to form $[Pb(TEA)]^{2+}$ in the absence of ammonia liquor. $[Pb(TEA)]^{2+}$ was then decomposed into Pb^{2+} and TEA under alkaline conditions. Finally, Pb^{2+} reacted with S^{2-} from reactions (2) and (3) to synthesize PbS on Si(100) wafers.

2.2 Characterization Techniques

The microstructure (i.e., crystalline structure and surface morphology) of the PbS films prepared were characterized with the use of X-ray diffraction (XRD) (Philips PANalytical X'Pert, $\lambda = 0.15405$ nm for CuKα radiation) and field-effect scanning electron microscopy (SEM, JSM-6060). Absorption spectra were obtained using UV visible near infrared (UV-VIS-NIR) spectrophotometer (Shimadzu Company, UV-3150). Film thickness was obtained using the cross-section SEM image and the film's elemental analysis was performed using an energy-dispersive spectrometer.

3 Results and Discussion

3.1 Crystalline Structure and Surface Morphology

Figure 1 shows the XRD patterns of all as-deposited film samples. The observed d-spacing and strong peaks that correspond to the diffraction of crystal faces (111), (200), (220), and (311) were in good agreement with the standard XRD data (Card no. 00-010-0448) regardless of the initial ingredients. The results indicated that all PbS films were polycrystalline with face-centered cubic (fcc) rock salt structures. Dominant and sharp peaks in XRD patterns revealed the good crystallinity of the films. A weak diffraction peak was observed at a Bragg angle of 35.7° because of the presence of impurities from the used precursors. XRD results suggested that PbS was stable, and its formation was rarely dependent on C_{Pb} and C_S. Table 2 lists the ratios of the integrated intensities of diffraction peaks (I_{111}/I_{200}) for all PbS films. I_{111}/I_{200} markedly increased from 0.88 to 1.28 with increased C_S and a fixed C_{Pb} of 0.5 M, implying the change in preferred orientation from <200> to <111>. The preferred <200> orientation was reported by Gadave [25] for CBD-deposited PbS films at 80 °C and by Puiso [26] for successive ionic layer adsorption and reaction (SILAR)-deposited PbS films on Si substrates. The preferred <111> was found by Remadevi [23] for SILAR-deposited PbS in neutral medium. I_{111}/I_{200} gradually decreased with increased C_S from 0.5 to 3.0 M and fixed C_{Pb} of 1.0 M. The result implied that the preferred <200> orientation was enhanced because of the low surface-free energy of the (200) crystal face and the crystallite growth on the (200) plane that suppressed the other crystal planes. The weak and enhanced <200> orientation was inherently related to the change in crystallite size and thickness of the PbS films. Given a fixed C_S, the preferred orientation of the film changed with C_{Pb}.

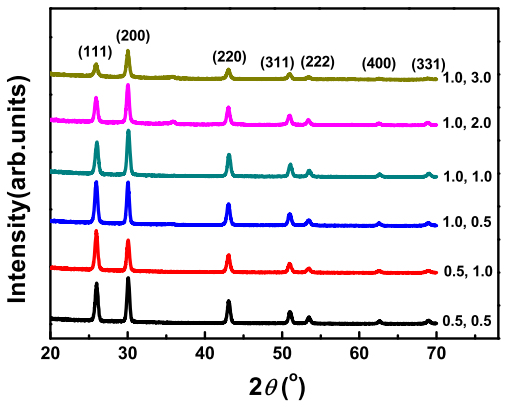

Fig. 1 XRD patterns of the PbS films using different C_{Pb} and C_S values

Table 2 Ratio of the I_{111} to I_{200} of the PbS films using different C_{Pb} and C_S values

C_{Pb}(M)	C_S(M)	I_{111} / I_{200}
0.5	0.5	0.88
0.5	1.0	1.28
1.0	0.5	1.01
1.0	1.0	0.75
1.0	2.0	0.68
1.0	3.0	0.55

The average crystallite size can be calculated from the XRD spectra by using the Debye-Scherrer formula as follows [27]:

$$D = 0.94\lambda/(\beta \cos\theta), \tag{5}$$

where λ is the x-ray wavelength, β is the full width at half maximum, and θ is the Bragg angle. Debye-Scherrer formula is widely used to calculate the average crystallite size less than 100 nm because the broadening of the diffraction peak caused by the stress can be negligible compared with that caused by the crystallite size at this time even though one can only have crude estimate of the average crystallite size by using the Debye-Scherrer formula. Apart from this approach, other procedures, such as the Rietveld method, that can also provide crystallite size. The Rietveld method is a structure refinement method and not a structure solution method. The Rietveld method is more suitable for a powder sample that is homogeneous in compositions and has a sufficient number of crystallite with random orientations. In this work, the crystallite size of the PbS film is anisotropic, i.e., the crystallite size strongly depends on the orientation. The Rietveld method is not suitable for the structural analysis of the PbS film samples. It is more suitable for calculating the crystallite size of the PbS films using Debye-Scherer formula. Table 3 shows the average crystallite sizes of PbS films for different C_{Pb} and C_S values along <111> and <200>. The average crystallite size varied from 20 to 74 nm for nanocrystalline films. The crystallite size along the <111> orientation initially decreased and then increased with C_S (critical C_S = 1.0 M) at fixed C_{Pb} of 1.0 M. By contrast, the crystallite size along the <200> orientation differed from that of the <111> orientation. The grain shape was far from spherical because of the anisotropy of the crystallite size of PbS films along different orientations. The change in crystallite size along <111> and <200> orientations could be associated with the concentration of precursors and film stress.

In our analysis, the constant a for cubic structures is given by the following expression:

$$a = d(h^2 + l^2 + k^2)^{1/2}, \tag{6}$$

Table 3 Calculated average crystallite sizes of the PbS films using different C_{Pb} and C_S values

C_{Pb}(M)	C_S(M)	Crystal orientation	D (nm)
0.5	0.5	<111>	20.2
		<200>	64.0
0.5	1.0	<111>	74.0
		<200>	22.4
1.0	0.5	<111>	55.5
		<200>	52.5
1.0	1.0	<111>	22.2
		<200>	56.8
1.0	2.0	<111>	23.2
		<200>	56.0
1.0	3.0	<111>	24.7
		<200>	20.4

where d is the interplanar distance of the crystal face (hkl). The lattice constants in terms of the maximum θ, albeit reasonably accurate, were found to be slightly dependent on θ. The result was attributed to the divergences of the refraction and absorption of x-ray beams by the specimens, which involved systematic errors in the measurement of θ and d [28]. Thus, the corrected value of lattice constants a' has been estimated from the Nelson-Riley plots [29]:

$$f(\theta) = [\cos^2\theta/\sin\theta + \cos^2\theta/\theta]/2 \quad (7)$$

The corrected value of a' is obtained by extrapolating the plot to $\theta = 90\,^\circ$. The Nelson-Riley plot for the PbS film using C_{Pb} and C_S values of 1.0 and 0.5 M is shown in Fig. 2. Table 4 shows the values of a' and lattice strain (δ) for PbS films at different C_{Pb} and C_S. δ is calculated using (8) as follows [30]:

$$\delta = (a_0 - a')/a_0, \quad (8)$$

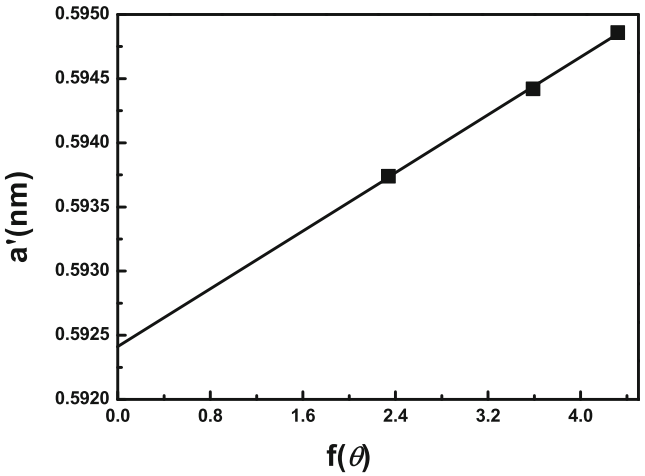

Fig. 2 Nelson-Riley plot for the PbS film using C_{Pb} and C_S values of 1.0 and 0.5 M

Table 4 The corrected value of lattice constants a' and lattice strain δ of the PbS films using different C_{Pb} and C_S values

C_{Pb}(M)	C_S(M)	a'(nm)	δ(%)
0.5	0.5	0.5932	0.034
0.5	1.0	0.5929	0.084
1.0	0.5	0.5923	0.185
1.0	1.0	0.5921	0.219
1.0	2.0	0.5928	0.101
1.0	3.0	0.5930	0.067

where a_0 is the lattice constant of the strain-free bulk PbS ($a_0 = 0.5934$ nm). Deviations of the calculated lattice parameter a' from a_0 indicated that the as-deposited films were under transverse compressive and tensile strain. It is found that δ of the PbS films initially increased and then decreased with increased C_S (critical $C_S = 1.0$ M). δ values for all the PbS films were larger than zero, suggesting that the crystal faces were under transverse tensile stress parallel to the interface. Nanoparticle strain was mainly induced by edge dislocations [31]. Changes in film stress with C_{Pb} and C_S affected the absorption of PbS films in the near-infrared region.

Figure 3 shows the SEM images of PbS films for different C_{Pb} and C_S. The film became sparse and the particle size decreased with increased C_S from 0.5 to 1.0 M and a fixed C_{Pb} of 0.5 M. The particles were pyramidal because of aggregate grains. Given the increased C_S from 0.5 to 3.0 M and a fixed C_{Pb} of 1.0 M, the film became dense, smooth, and homogeneous. The particle size initially increased and decreased. Moreover, the film comprised irregular particles. Increased C_S at fixed C_{Pb} enhanced the formation of PbS, which explained the evolution of the surface morphologies of the film. C_{Pb} was relatively reduced and insufficient when C_S exceeded a specific value. In addition, Pb^{2+} could not combine with all the S^{2-}. The surface of the PbS films became dense with increased C_{Pb} at $C_S = 1.0$ M. Figure 4 shows the behavior of the thickness of the PbS films with increased C_S at $C_{Pb} = 1.0$ M. The film thickness increased from 261.0 to 405.9 nm with increased C_S (critical $C_S = 2.0$ M); the thickness of the PbS films initially increased and decreased. The increased film thickness with C_S was mainly attributed to the accelerated formation of PbS. Meanwhile, the reduced film thickness with C_S was caused by the increased film density.

Table 5 presents the elemental atomic percentages of the films with $C_S = 0.5$, 1.0, 2.0, and 3.0 M. The Si element was from the Si substrate. No other impurities were detected, confirming the high purity of the PbS film. The ratio of the atomic percentages of S to Pb initially increased and then decreased with increased C_S. The initial increase suggested that several PbS compounds were formed with increased

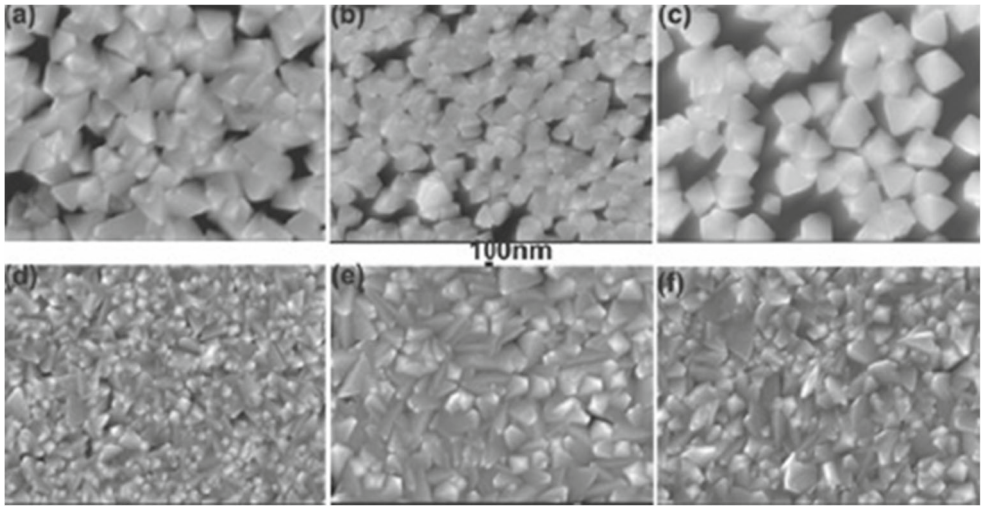

Fig. 3 SEM images of the PbS films using C_{Pb} and C_S values of **a** 0.5, 0.5; **b** 0.5, 1.0; **c** 1.0, 0.5; **d** 1.0, 1.0; **e** 1.0, 2.0; **f** 1.0, 3.0 M

C_S, whereas the subsequent reduction was caused by the depletion of Pb^{2+} ions. All PbS films were Pb-sufficient, in which the sufficiency initially decreased and then increased with C_S.

3.2 Near-Infrared Absorption

Modification of the optical band gap is critical for semiconductor materials. The optical band gap is calculated from the spectral absorption near the fundamental absorption edge. The direct band gap of all synthesized PbS films was estimated using the Tauc relation given as follows [32]:

$$\alpha \propto (h\nu - E_{opt})^n, \tag{9}$$

where α is the absorption coefficient, $h\nu$ is the photon energy, and E_{opt} is the optical band gap. The index n characterized the nature of band transition between the valence and conduction bands; $n = 1/2$ and 2 for direct and indirect band gap semiconductors, respectively. Figure 5 plots α^2 against $h\nu$ for the PbS film with $C_{Pb} = C_S = 1.0$ M, in which the inset represents the absorption spectrum of the film. All the samples exhibited gradually increased absorption from the near-infrared region to the visible region. The increase in absorption was attributed to the transition of electrons from valence band to conduction band [23]. Band gap energies could be estimated by extrapolating the linear portion of the graph to the $h\nu$ axis. The band gap energy of the PbS film was 1.32 eV ($\lambda = 939.39$ nm) for $C_{Pb} = C_S = 1.0$ M, which was consistent with reported results [33]. Our findings demonstrated that the synthesized PbS film was a narrow direct band gap semiconductor. The same method could be used to obtain the absorption edges of the films ranging from 0.92 to 1.32 eV as shown in Table 6. The absorption edge of the film slightly blueshifted with increased C_{Pb}. Meanwhile, the absorption edge of the films initially blueshifted and then redshifted with increased C_S (critical $C_S = 1.0$ M). For synthesized PbS films, the blueshifted absorption edge was attributed to the initial increase in δ; the tensile stress of the films increased with increased C_S to 1.0 M. However, the redshifted absorption edge was related to the reduced tensile stress of the films. The increased particle size also affected the absorption edge of PbS films and reduced the band gap (i.e., redshifted).

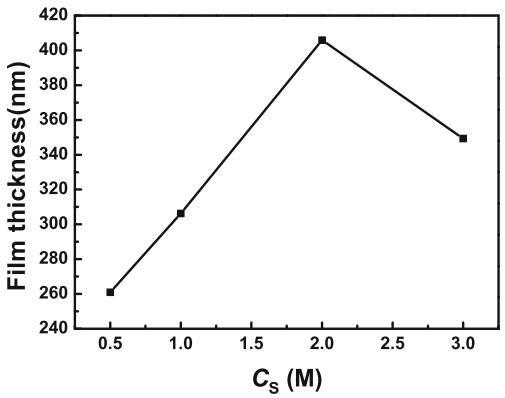

Fig. 4 Thickness of the PbS films with increased C_S at $C_{Pb} = 1.0$ M

Table 5 Elemental atomic percentages of the PbS films with different C_S values

C_S(M)	Si (%)	S (%)	Pb (%)	S/Pb
0.5	90.04	4.51	5.45	0.82
1.0	85.68	6.66	7.65	0.87
2.0	66.57	16.36	17.07	0.96
3.0	67.17	14.16	18.67	0.76

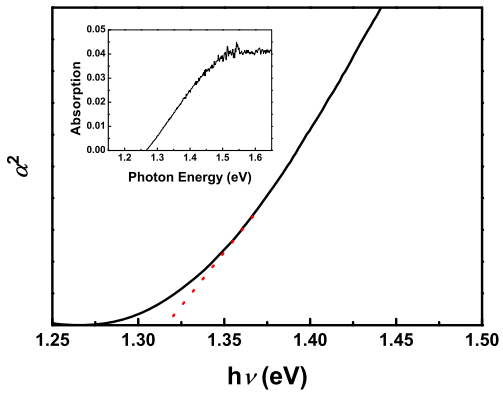

Fig. 5 $\alpha^2(h\nu)$ plot for the PbS film with $C_{Pb} = C_S = 1.0$ M

Table 6 Calculated absorption edges of the PbS films using different C_{Pb} and C_S values

C_{Pb}(M)	C_S(M)	E_{opt} (eV)
0.5	0.5	0.92
0.5	1.0	1.16
1.0	0.5	1.03
1.0	1.0	1.32
1.0	2.0	1.05
1.0	3.0	0.95

4 Conclusion

Nanocrystalline PbS films with fcc structures were successfully prepared on p-type Si (100) wafers through CBD method using various C_{Pb} and C_S. The density and average particle size of the PbS films increased at $C_{Pb} = 1.0$ M. The film surfaces were smoothened with increased C_S from 0.5 to 2.0 M. However, the particle size was reduced with further increase in C_S. The absorption edge of the films based on Tauc formula ranged from 0.92 to 1.32 eV. The absorption edge of the films slightly blueshifted with increased C_{Pb}; by contrast, the absorption edge initially blueshifted and then redshifted with increased C_S at $C_{Pb} = 1.0$ M. The blueshifted absorption edge was attributed to the initial increase in δ of the films with increased C_S to 1.0 M. However, the redshifted absorption edge was related to the decreased tensile stress of the samples.

Acknowledgments I'm grateful for the supports from the National Natural Science Foundation of China (grant no. 60807001), the Foundation of Young Key Teachers from University of Henan Province (Grant no. 2011GGJS-008) and the Foundation of Henan Educational Committee (Grant no. 2010A140017).

References

1. S. Mitra, A. Mandal, S. Banerjee, A. Dutta, S. Bhattacharya, A. Bose, D. Chakravorty, Indian J. Phys. **85**, 649 (2011)
2. S. Tekerek, A. Kudret, U. Alver, Indian J. Phys. **85**, 1469 (2011)
3. G. Mandal, T. Ganguly, Indian J. Phys. **85**, 1229 (2011)
4. J. Bhadra, D. Sarkar, Indian J. Phys. **84**, 693 (2010)
5. A.U. Ubale, A.N. Bargal, Indian J. Phys. **84**, 1497 (2010)
6. C.D. Lokhande, A.U. Ubale, P.S. Patil, Thin Solid Films **1**, 302 (1997)
7. R.K. Joshi, K. Aloke, H.K. Sehgal, Appl. Surf. Sci. **221**, 43 (2004)
8. H. Moreno-Garcia, M.T.S. Nair, P.K. Nair, Thin Solid Films **519**, 2287 (2011)
9. S. Seghier, N. Kamoun, R. Brini, A.B. Amara, Mater. Chem. Phys. **97**, 71 (2006)
10. A. Osherov, J.P. Makai, J. Balazs, Z.J. Horvath, N. Gutman, A. Sa ar, Y. Golan, J. Phys.-Condens. Mat. **22**, 262002 (2010)
11. P.K. Nair, V.M. Garcia, A.B. Hrenandez, M.T.S. Nair, J. Phys. D: Appl. Phys. **24**, 1466 (1991)
12. S. Kumar, T.P. Sharma, M. Zulfequar, M. Husain, Physica B **325**, 8 (2003)
13. J. Muscat, J.D. Gale, Geochim. Cosmochim. Ac. **67**, 799 (2003)
14. K.K. Nanda, F.E. Kruis, H. Fisan, J. Appl. Phys. **91**, 2315 (2002)
15. D. Li, C.J. Liang, Y. Liu, S.X. Qian, J. Lumin. **122**, 549 (2007)
16. A.P. Gaiduk, P.I. Gaiduk, N.L. Arne, Thin Solid Films **516**, 3791 (2008)
17. Y. Badr, M.A. Mahmond, Physica B **388**, 134 (2007)
18. M. Sharon, K.S. Ramaiah, K. Mukul, N.S. Michael, L.C. Claude, Chem. Electroanal. **436**, 49 (1997)
19. Y.H. Ni, F. Wang, H.J. Liu, G. Yin, J.M. Hong, X. Ma, Z.J. Xu, Growth Cryst. **262**, 399 (2004). (in Chinese)
20. Y. Zhao, X.H. Liao, J.M. Hong, J.J. Zhu, Mater. Chem. Phys. **87**, 149 (2004). (in Chinese)
21. E. Pentia, L. Pintilie, C. Tivarus, I. Pintilie, T. Botila, Mater. Sci. Eng. B **80**, 23 (2001)
22. J.J. Valenzuela-Jauregui, R. Ramirez-Bon, A. Mendoza-Galvan, M. Sotelo-Lerma, Thin Solid Films **441**, 104 (2003)
23. T.L. Remadevi, K.C. Preetha, Mater. Electron. **23**, 2017 (2012)
24. K.C. Preetha, T.L. Remadevi, Mater. Electron. **24**, 489 (2013)
25. K.M. Gadave, S.A. Jodgudri, C.D. Lokhande, Thin Solid Films **245**, 7 (1994)
26. J. Puiso, S. Tamulevicius, G. Laukaitis, S. Lindross, M. Leskeia, V. Snitka, Thin solid Films **403**, 457 (2002)
27. B.D. Cullity, *Elements of x-ray diffraction*, 2nd edn (Addison-Wesley publishing co. Inc, London, 1978), p. 327
28. A. Hussain, A. Begum, A. Rahman, Arab. J. Sci. Eng. **38**, 169 (2013)
29. E. Lifshin, *X-ray characterization of materials* (Wiley, New York, 1999), p. 37
30. N. Choudhury, B.K. Sarma, Bull. Mater. Sci. **32**, 43 (2009)
31. M.P.C. Kalita, K. Deka, J. Das, N. Hazarika, P. Dey, Mater. Lett. **87**, 84 (2012)
32. J. Tauc, *Amorphous and liquid semiconductor* (Plenum, New York, 1974), p. 159
33. P. Srinivasan, P. Rajesh, Thin film technology **42**, 6206 (2012)